Title: Corrosion study of resorbable Ca60Mg15Zn25 bulk metallic glasses in physiological fluids

Author: Rafał Babilas, Anna Bajorek, Adrian Radoń, Ryszard Nowosielski

Citation style: Babilas Rafał, Bajorek Anna, Radoń Adrian, Nowosielski Ryszard. (2017). Corrosion study of resorbable Ca60Mg15Zn25 bulk metallic glasses in physiological fluids. "Progress in Natural Science: Materials International" (Vol. 27, iss. 5 (2017), s. 627-634), doi 10.1016/j.pnsc.2017.08.011

Progress in Natural Science: Materials International 27 (2017) 627–634

HOSTED BY

Contents lists available at ScienceDirect

Progress in Natural Science: Materials International

journal homepage: www.elsevier.com/locate/pnsmi

Original Research

Corrosion study of resorbable $Ca_{60}Mg_{15}Zn_{25}$ bulk metallic glasses in physiological fluids

Rafał Babilas[a,*], Anna Bajorek[b], Adrian Radoń[a], Ryszard Nowosielski[a]

[a] Institute of Engineering Materials and Biomaterials, Silesian University of Technology, Konarskiego 18a St., 44-100 Gliwice, Poland
[b] A. Chelkowski Institute of Physics, University of Silesia, Uniwersytecka 4 St., 40-007 Katowice, Poland

ARTICLE INFO

Keywords:
Ca-based metallic glasses
X-ray photoelectron spectroscopy
FTIR spectroscopy
X-ray diffraction
Corrosion resistance
Hydrogen evaluation

ABSTRACT

The corrosion activity of amorphous plates of $Ca_{60}Mg_{15}Zn_{25}$ alloy was investigated. The biocompatible elements were selected for the alloy composition. The electrochemical corrosion and immersion tests were carried out in a multi-electrolyte fluid and Ringer's solution. Better corrosion behavior was observed for the samples tested in a multi-electrolyte fluid despite the active dissolution of Ca and Mg in Ringer's solution. The experimental results indicated that reducing concentration of NaCl from 8.6 g/dm^3 for Ringer's solution to 5.75 g/dm^3 caused the decrease of the corrosion rate. The volume of the hydrogen evolved after 480 min in Ringer's solution (40.1 ml/cm^2) was higher in comparison with that obtained in a multi-electrolyte fluid (24.4 ml/cm^2). The values of open-circuit potential (E_{OCP}) for the $Ca_{60}Mg_{15}Zn_{25}$ glass after 1 h incubation in Ringer's solution and a multi-electrolyte fluid were determined to be −1553 and −1536 mV vs. a saturated calomel electrode (SCE). The electrochemical measurements indicated a shift of the corrosion current density (j_{corr}) from 1062 μA/cm^2 for the sample tested in Ringer's solution to 788 μA/cm^2 for the specimen immersed in a multi-electrolyte fluid. The corrosion products analysis was conducted by using the X-ray photoelectron spectroscopy (XPS). The corrosion products were identified to be $CaCO_3$, $Mg(OH)_2$, CaO, MgO and ZnO. The mechanism of corrosion process was proposed and described based on the microscopic observations. The X-ray diffraction and Fourier transform infrared spectroscopy (FTIR) also indicated that $Ca(OH)_2$, $CaCO_3$, $Zn(OH)_2$ and $Ca(Zn(OH)_3)_2{\cdot}2H_2O$ mainly formed on the surface of the studied alloy.

1. Introduction

In recent years, great efforts have been aimed to Ca-based metallic glasses due to their biocompatibility and resorbable properties. Calcium alloys can be assumed as potential biomaterials for artificial implants. Moreover, these materials have a low density and do not have negative influences on the human body [1–5].

The first report about ternary Ca-Mg-Zn bulk metallic glasses were introduced in 2004 by Senkov and Scott [6], who produced several Ca-Mg-Zn alloys by a copper mold casting method. The alloy compositions were selected using specific criteria that the large atomic radius of Ca is taking into account [7]. That radius increases a glass-formation ability and a low density of Ca, which may be useful for development of light alloys [8,9]. Moreover, alloying additions like Mg and Zn should form a deep eutectic with Ca, which is important for achieving glassy materials [10,11]. Basing on mentioned rules Senkov et al. proposed Ca-based compositions of $Ca_{55}Mg_{15+x}Zn_{30-x}$ (x = 0, 5, 10), $Ca_{60}Mg_{10+y}Zn_{30-y}$ (y = 0, 5, 7.5, 10) and $Ca_{55+z}Mg_{25-z}Zn_{20}$, (z = 0, 5, 7.5, 10, 15), which critical casting thicknesses vary from 0.5 up to 10 mm [12].

Unfortunately, using of calcium alloys as biomaterials are limited by their low corrosion resistance. Some papers [13–15] reported that the corrosion rate of calcium alloys is relatively rapid. It is also known that the degradation of calcium alloys leads to the hydrogen evolution. Moreover, a negative corrosion reaction of this material in distilled water was able to decompose into the corrosion products mainly contained of calcium oxides and calcium hydroxides.

Despite of this, more tests and studies should be provided to further examination of biocorrosion activity of glassy Ca-based alloys. In some cases, the corrosion activity of calcium alloys may be decreased by the introduction of alloying elements. Li et al. [16] stated that the degradable and dissoluble features of Ca-Mg-Zn glasses in pure water can be controlled by changing the composition and alloying additions (i.e. lithium component). Rau et al. [17] also proposed that the rate of biodegradation of Ca-based glasses in human body should be limited by using glass-ceramic coatings introduced on the surface of the sample. In order to decrease the corrosion rate of calcium glasses Li et al. [5]

Peer review under responsibility of Chinese Materials Research Society.
* Corresponding author.
E-mail address: rafal.babilas@polsl.pl (R. Babilas).

http://dx.doi.org/10.1016/j.pnsc.2017.08.011
Received 3 January 2017; Received in revised form 2 August 2017; Accepted 21 August 2017
Available online 29 September 2017

prepared anti-corrosive protection to Ca-Mg-Zn alloys including iron films, fluoroalkylsilane coatings and bilayer of iron films with fluoroalkylsilane coatings.

The aim of the research presented herein is to study the effect of corrosive environment, which contains selected salts, on the active behavior of bulk Ca-based metallic glass. The $Ca_{60}Mg_{15}Zn_{25}$ glassy plates can be expected as the bioresorbable materials due to consisting of the biocompatible elements - Ca, Mg and Zn. In this study a commercial multi-electrolyte fluid and Ringer's solutions were used as isotonic solutions related to the simulated body fluids. These fluids are often used in many "in vitro" experiments on organs and tissues. The corrosion rate of glassy samples was determined by the hydrogen evolution testing and polarization measurements. The corrosion products formed on a surface of the glassy samples after immersion tests were described in detail by X-ray photoelectron spectroscopy, Fourier transform infrared spectroscopy and conventional X-ray diffraction. Moreover, the changes of surface in a function of immersion time were also observed using a light microscopy.

2. Experimental

A master alloy with the composition of $Ca_{60}Mg_{15}Zn_{25}$ (at%) was fabricated in an induction furnace using pure elements (99.9%) under the protection of argon atmosphere. The ingot was remelted several times to ensure that the alloy composition was homogeneous. The samples in the form of plates with a length and a width of 10 mm and a thickness of 1 mm were produced by the high-pressure die casting [18–20].

The amorphous nature of the samples in the as-quenched state and phase identification of the samples after immersion was studied by the X-ray diffraction (XRD) in the reflection mode using the diffractometer with conventional Co *K*α radiation source. The glassy state was also confirmed by differential scanning calorimetry (DSC) at a constant heating rate of 20 K/min under the argon atmosphere. The DSC method was allowed to determine the crystallization temperature and glass-stability of the samples.

The corrosion activity determined by a hydrogen evaluation was studied by immersion tests in Baxter multi-electrolyte fluid (5.75 g/dm^3 NaCl, 0.38 g/dm^3 KCl, 0.394 g/dm^3 $CaCl_2{\cdot}6H_2O$, 0.2 g/dm^3 $MgCl_2{\cdot}6H_2O$, 4.62 g/dm^3 $CH_3COONa{\cdot}3H_2O$, 0.9 g/dm^3 $C_6H_5Na_3O_7{\cdot}2H_2O$) and Baxter Ringer's solution (8.6 g/dm^3 NaCl, 0.3 g/dm^3 KCl, 0.48 g/dm^3 $CaCl_2{\cdot}6H_2O$). The tests were carried out at 37 °C in function of time by using experimental set up described in the reference [21]. Ringer's solution and a physiological fluid are often used in medicine (in the form of the infusion) as medium for irrigation and complementary deficiency of electrolytes.

The electrochemical measurements were conducted in a typical three-electrode cell using a sample as working electrode, a saturated calomel electrode (SCE) as reference electrode and a platinum counter electrode presented in [22]. The corrosion resistance was evaluated by recording of the open-circuit potential (E_{OCP}) variation and potentiodynamic polarization curves in the potential range E_{OCP} − 250 mV to E_{OCP} + 250 mV. The corrosion potential (E_{corr}), corrosion current density (j_{corr}) and polarization resistance (R_p) was also determined by the Tafel and Stern-Geary method [23]. The samples were measured from a near-steady-state corrosion potential after a period of open-circuit potential stabilization. The E_{OCP} was monitored for 3600 s for each sample.

XPS measurements after immersion tests were carried out in PHI 5700/660 Physical Electronics spectrometer under the ultrahigh vacuum conditions (10^{-10} Torr) by using monochromatic Al Kα X-ray source with the energy 1486.6 eV. Before measurements all the samples were kept under vacuum of 10^{-9} Torr for 7 days. All the performed spectra were determined relative to the C1s peak (BE = 284.8 eV) as an adventitious carbon usually accumulated on the surface of the sample and used as a reference for charge correction. The analysis of collected data was made by using MultiPak 9.2 program basing on procedure described in work [24].

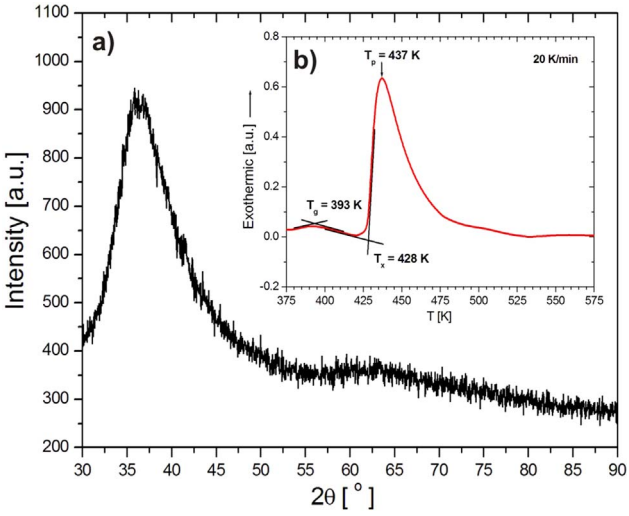

Fig. 1. XRD and DSC patterns of $Ca_{60}Mg_{15}Zn_{25}$ alloy in as-cast state.

Attenuated total reflectance Fourier transform infrared spectroscopy (ATR-FTIR) was acquired using the Thermo Scientific Nicolet 6700/8700 FT-IR spectrometer at the range of 400–4000 cm^{-1}. The spectra were collected by co-adding 300 scans. The baseline adjustment and smoothing was also provided.

The changes of surface morphology of the samples during 5 h of corrosion tests were analyzed using a light microscope (LM). Moreover, the changes of surfaces in function of immersion time were also observed by using an optical microscopy.

3. Results and discussion

Fig. 1a shows the X-ray diffraction pattern of $Ca_{60}Mg_{15}Zn_{25}$ alloy cast in the form of plate. The typical pattern for Ca-based metallic glasses [6,9,12] was obtained. The broad scattering signal centered at about 36° 2-theta angle is mainly shown. The XRD result confirmed an amorphous structure without detectable peaks, which may come from crystalline phases. Similarly to Wang et al. [14] the calorimetry measurements were done to determine the amorphous stability of the alloy. The corresponding DSC curve of the glass with obvious crystallization effect was presented in Fig. 1b. The exothermic peak is allowed to determine the onset (T_x) and peak crystallization (T_p) temperatures. The T_x and T_p are found to be 428 and 437 K, adequately. The DSC trace also exhibited the endothermic effect corresponding to the glass-transition temperature (T_g = 393 K). The supercooled liquid region ΔT_x (T_x - T_g) is about 35 K.

The E_{OCP} traces as a function of immersion time for glassy plates treated in a multi-electrolyte fluid and Ringer's solution at 37 °C are shown in Fig. 2a. As can be seen, the E_{OCP} value shifts towards the positive potential during a period of about the first 1500 s. It remains rather stable until the end of the test. The plate tested in a multi-electrolyte fluid exhibited more positive E_{OCP} value than that of glass after immersion in Ringer's solution. The final value of the E_{OCP} for studied alloy after 60 min of examination in Ringer's solution and a multi-electrolyte fluid was noticed to be −1553 and −1536 mV vs. SCE, adequately.

Based on the results presented by Niu et al. [25] we can state that a stabilization of the E_{OCP} value suggests that a passive film can be formed during the first 1 h of the immersion. In this case the film formation should act as a barrier for alloy dissolution and reducing the corrosion rate. Nevertheless, the Ca-based alloys as rapidly reactive and possibly initial passivation of the samples during first hour is not stable. The decrease of the open-circuit potential at the end of

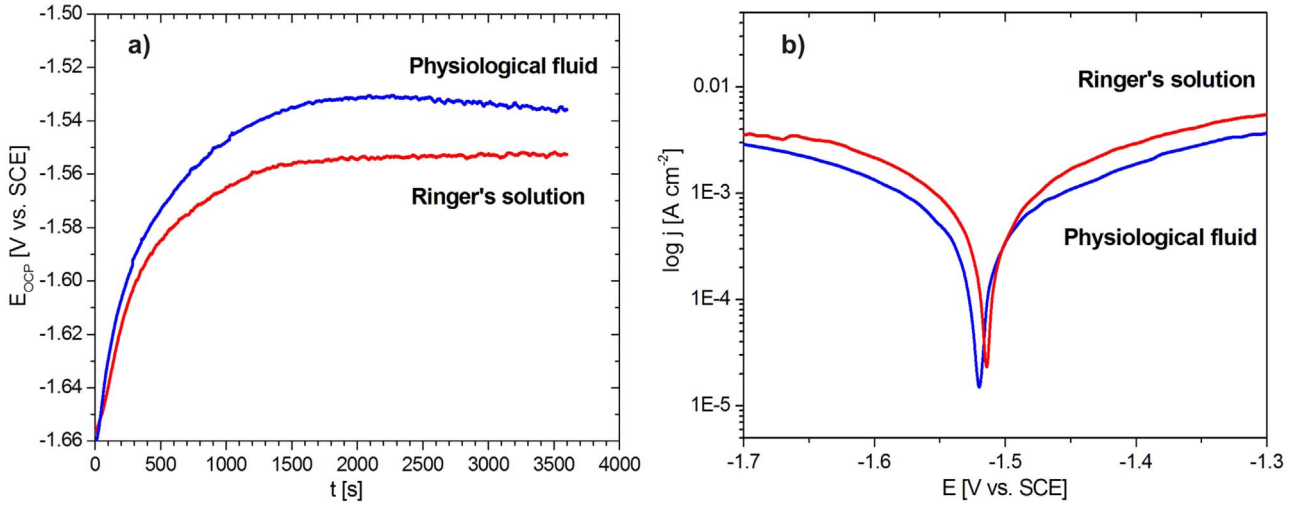

Fig. 2. Variation of the open-circuit potential with time (a) and polarization curves (b) for $Ca_{60}Mg_{15}Zn_{25}$ glasses in a multi-electrolyte fluid and Ringer's solution at 37 °C.

immersion time indicating further dissolution of the sample by a penetration of the solution into the film pores. The progressing corrosion behavior is seen during a next hours of immersion.

The typical potentiodynamic polarization curves of the samples in Ringer's solution and a multi-electrolyte fluid at 37 °C are shown in Fig. 2b. The polarization curves of the samples immersed in different solutions show a similar profile. The studied samples show higher polarization resistance and lower corrosion current density in a multi-electrolyte fluid. Some important data including the open-circuit potential (E_{OCP}), corrosion current density (j_{corr}), corrosion potential (E_{corr}) and polarization resistance (R_p) are summarized in Table 1. The j_{corr} of the plates examined in a multi-electrolyte fluid and Ringer's solution are 788 μA/cm^2 and 1062 μA/cm^2, adequately. The E_{corr} value is very similar for both samples, however better value was obtained after electrochemical tests in Ringer's solution. The polarization resistance changes from 0.21 kΩcm^2 for Ringer's solution to 1.22 kΩcm^2 for a multi-electrolyte fluid, respectively.

The poor corrosion resistance of Ca-based glasses was also noticed by Senkov et al. The electrochemical examinations of Ca-Mg-Zn bulk metallic glasses and crystalline Mg-Zn-Zr alloy (ZK60) in a 0.05 M Na_2SO_4 electrolyte were reported in [26,27]. The polarization curves for Ca-Mg-Zn bulk glassy materials and ZK60 alloy revealed that Ca-based glass and Mg-based crystalline alloy were active. However, the Cu addition to Ca-Mg-Zn composition can be allowed to achieve a slight passivity. The authors concluded that the electrochemical corrosion resistances of Ca-Mg-Zn glassy alloys with the Cu addition are comparable in some cases to Fe-based glasses and Mg-based crystalline alloys.

Fig. 3a shows the influence of testing media on the hydrogen evolution volume of $Ca_{60}Mg_{15}Zn_{25}$ glass as a function of time. The immersion tests were conducted in a multi-electrolyte fluid and Ringer's solution at 37 °C during 480 min. The tested samples of Ca-based glass exhibited significantly less hydrogen evolution volumes in a multi-electrolyte fluid (24.4 ml/cm^2) than in Ringer's solution (40.1 ml/cm^2). The result indicates that Ringer's solution is more aggressive. The growing tendency of evolved hydrogen as a function of

Table 1
Results of corrosion investigations of $Ca_{60}Mg_{15}Zn_{25}$ metallic glasses in a multi-electrolyte fluid and Ringer's solution (E_{OCP} - open-circuit potential, E_{corr} - corrosion potential, R_p - polarization resistance, j_{corr} - corrosion current density).

Sample	E_{OCP} [mV]	E_{corr} [mV]	R_p [kΩcm^2]	j_{corr} [μA/cm^2]
Ringer's solution	−1553 ± 36	−1514 ± 30	0.21 ± 0.01	1062 ± 45
Multi-electrolyte fluid	−1536 ± 33	−1520 ± 31	1.22 ± 0.05	788 ± 32

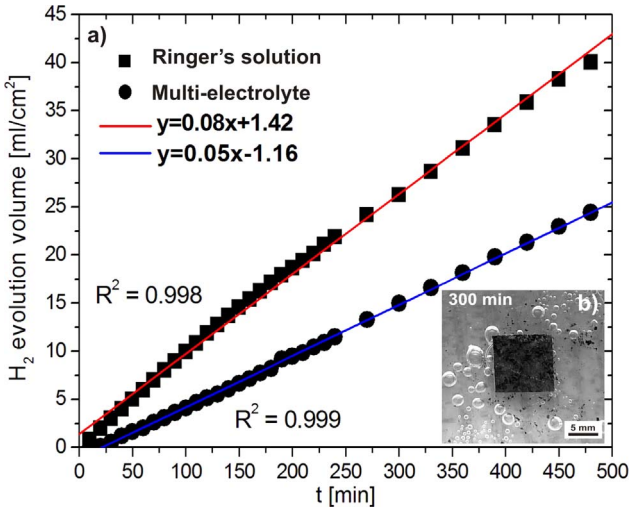

Fig. 3. Hydrogen evolution volume as an function of the immersion time in a multi-electrolyte fluid and Ringer's solution 37 °C (a) with changes of the surface morphology of plate after 300 min in Ringer's solution (b).

immersion time was also observed. The linear fitting of obtained data was provided to describe increasing tendency of H_2 evolution.

The observations of the surface morphology during immersion tests correspond with mentioned above studies of the hydrogen volume and confirm that the calcium-based alloys are an extremely reactive and spontaneously reacts with water generating hydrogen. After 300 min of immersion the rapid evolution of H_2 is seen (Fig. 3b). The large bubbles of hydrogen can be observed and corrosion products are removed from the sample surface.

In case to better describing of the post corrosion state of the glasses, the XPS measurements were used to determine the chemical composition of the corrosion products formed on the surface after immersion tests during 1 h. The XPS survey spectra collected at room temperature for glassy samples tested in two corrosion solutions after 1 h of immersion are presented in Fig. 4. All the characteristic peaks were denoted as C1s, O1s, Mg1s, Ca2p and Zn2p. In both cases the domination of oxygen and carbon accumulated on the surface was observed and these elements obviously varied upon sputtering.

Fig. 5a shows the atomic concentration estimated in DP-XPS mode of studied alloy for a multi-electrolyte fluid during 350 min of sputtering. The amount of oxygen was rather stable and varied only about less than 5 at%. The carbon accumulated on the sample surface drastically decreased with sputtering. The calcium dominated during the sputter

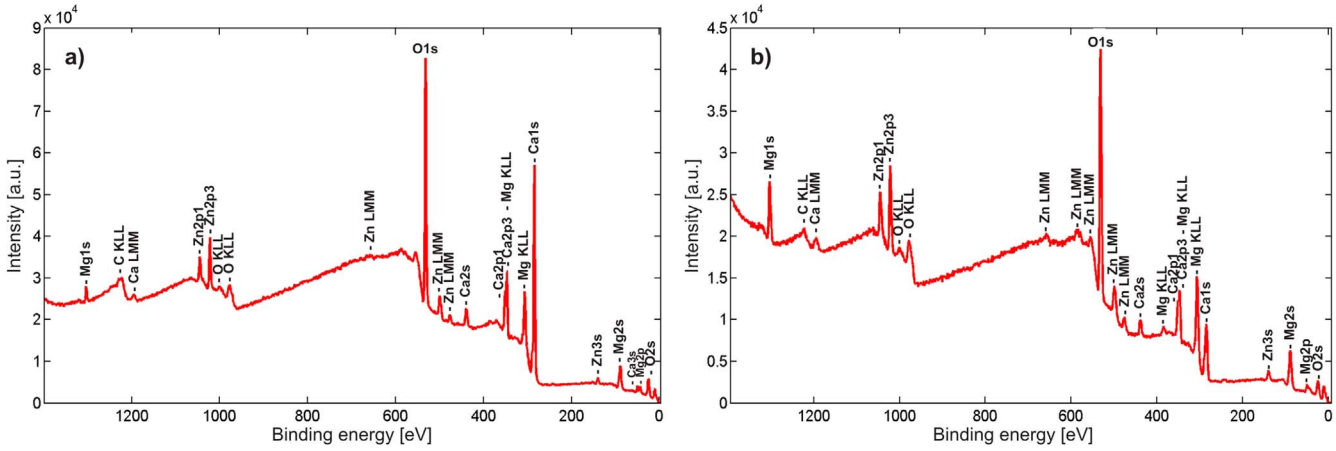

Fig. 4. XPS survey spectrum for $Ca_{60}Mg_{15}Zn_{25}$ alloy after corrosion test in a multi-electrolyte fluid (a) and Ringer's solution (b) after 1 h.

time and reached a value of 34 at%. The amount of magnesium was rather less than 8 at% and zinc was less than 3 at%.

By analyzing the individual core level lines upon sputtering some chemical states can be described (Fig. 6a-e). The carbon exhibits two separate peaks. Higher of them at lower binding energy (BE = 284.8 eV) may belong to the carbon, while the second one may be rather connected to some carbonates adsorbed on the sample surface (Fig. 6a). The oxygen line is rather stable and can be related directly to the $CaCO_3$ states (BE = 531.4 eV), but after third run of sputtering when the magnesium reaches similar level as calcium, this lower BE peak may be rather associated to presence of $Mg(OH)_2$ (BE = 530.9 eV) as a part of the O1s broad peak (Fig. 6b). The calcium 2 s line can be related to CaO (Fig. 6c). The magnesium line exhibits two components. The first one at lower binding energy range is associated to the Ca3s line (BE = 50.8 eV) as calcium oxide and the second at higher BE is Mg2p line, which is dependent on the sputtering stage. Initially, we can observe mostly the $Mg(OH)_2$ line (BE = 49.5 eV), whereas it can be transformed into the MgO (BE = 50.8 eV) during sputtering process. Thus at the final stage of sputtering we have mostly MgO instead of pure Mg (Fig. 6d). The zinc 2p line shows LS splitting into $2p_{3/2}$ and $2p_{1/2}$, which slightly changes upon sputtering and equals about $\Delta E_B \approx$ 23.15 eV (Fig. 6e). The binding energy for Zn line is typical as for the ZnO ($Zn2p_{3/2}$, BE = 1021.75 eV). To sum up, the chemical states of individual core level lines are strongly dependent on used corrosive environment for sample treatment.

Fig. 5b presents the result of DP-XPS measurements performed during 350 min of sputtering for the glassy sample in Ringer's solution. A slight variation of oxygen concentration upon sputtering time can be noticed, which value was still maintain above 55 at%. Carbon exhibits a significant drop just in the first step of sputtering due to the removal of carbon adsorbed on the surface. Simultaneously, calcium, magnesium and zinc show a slight increase. The calcium reached a value of 21 at%, Zn almost 16 at%, but Mg was lower than 7 at%.

The analysis of individual core level lines upon sputtering for sample tested in Ringer's solution is also provided (Fig. 6f-j). Similarly to the above results for a physiological fluid, carbon exhibits two separate peaks (Fig. 6f). The oxygen indicates two lines. This one with higher BE may be related to the ZnO states (BE = 530.4 eV) and the second with lower binding energy (BE =529.4 eV) is typical for the CaO states (Fig. 6g). The influence of Mg on the oxygen line is rather low due to the fact, that the amount of Mg is relatively lower than Ca and Zn. The core level Ca2p line is a typical line for the CaO states (BE = 346.1 eV). The separation between two Ca2p components varies upon sputtering. Thus, for some stage of DP we can see well separated 2p lines whereas just after two runs both lines are slightly overlapped each other (Fig. 6h). The magnesium line is dependent on the sputtering stage. At the beginning, we can notice mostly the $Mg(OH)_2$ line (BE = 49.5 eV), whereas it can be changed into MgO (BE = 50.8 eV). At the final stage of sputtering we obtained the MgO instead of pure Mg (Fig. 6i). The zinc 2p line shows double line due to the LS splitting into $2p_{3/2}$ and $2p_{1/2}$, which only slightly varied upon sputtering and reached a value about $\Delta E_B \approx$ 23.11 eV (Fig. 6j).

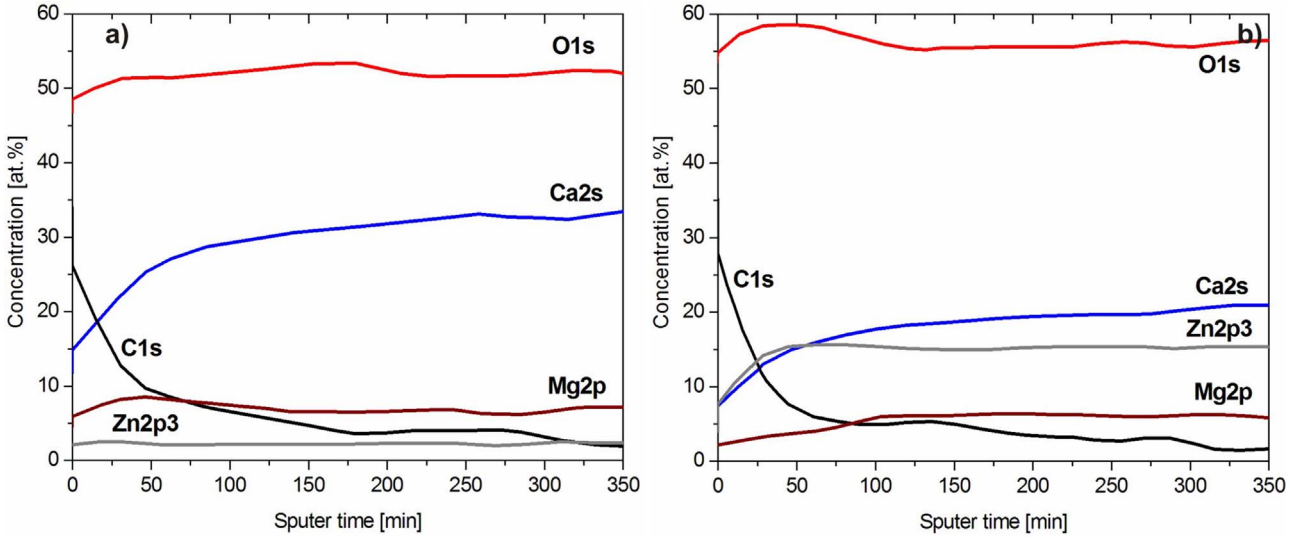

Fig. 5. XPS depth profiles for $Ca_{60}Mg_{15}Zn_{25}$ alloy after corrosion test in a multi-electrolyte fluid (a) and Ringer's solution (b).

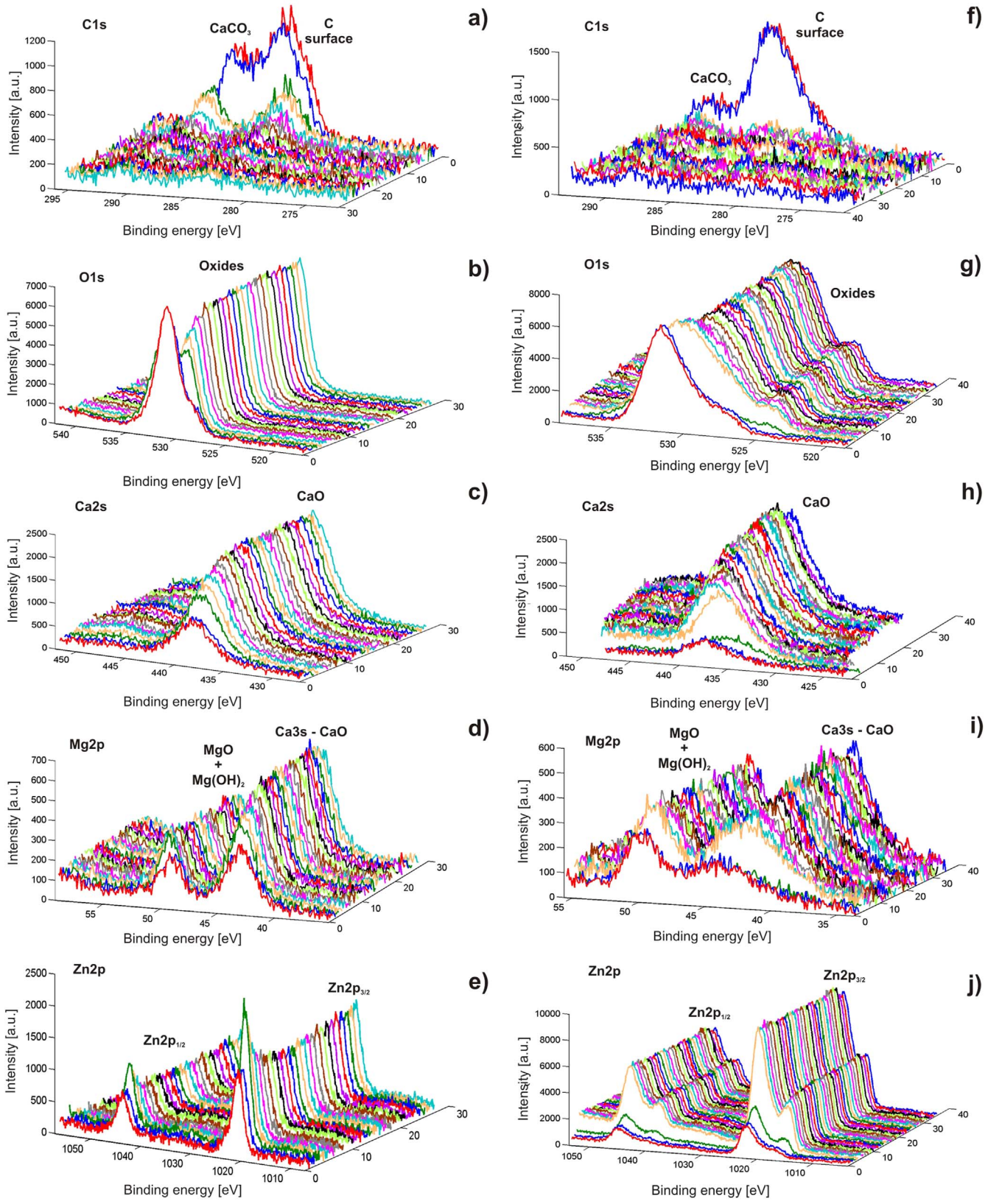

Fig. 6. XPS narrow scan spectra of C1s (a, f), O1s (b, g), Ca2s (c, h), Mg2p (d, i), Zn2p (e, j) for $Ca_{60}Mg_{15}Zn_{25}$ alloy after corrosion test in a multi-electrolyte fluid (a-e) and Ringer's solution(f-j).

Nonetheless, the $Zn2p_{3/2}$ line was composed of two lines. This one with higher intensity may be ascribed as a line typical for the ZnO ($Zn2p_{3/2}$, BE = 1021.75 eV).

The X-ray analysis (Fig. 7) of the corrosion products of studied samples after 1 h of immersion tests in a multi-electrolyte fluid and Ringer's solution identified the calcium hydroxide ($Ca(OH)_2$), the calcium carbonate ($CaCO_3$), the zinc hydroxide ($Zn(OH)_2$) and the calcium zinc hydroxide hydrate ($Ca(Zn(OH)_3)_2{\cdot}2H_2O$). For compari-

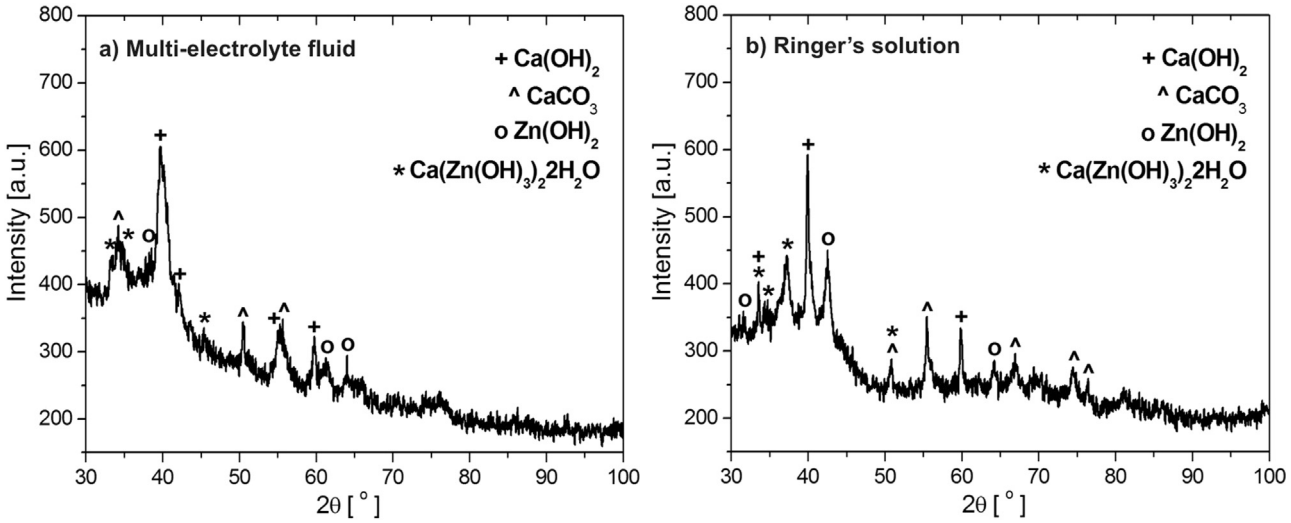

Fig. 7. XRD patterns of the corrosion products after 1 h of immersion in a multi-electrolyte fluid (a) and Ringer's solution (b).

son, Dahlman et al. [15] used the XRD analysis for an identification of the corrosion products in the form of powder collected from $Ca_{65}Mg_{15}Zn_{20}$ glassy sample after a static aqueous submersion at room temperature. The XRD measurements is allowed to identify the calcium hydroxide ($Ca(OH)_2$), the calcium zinc hydroxide hydrate ($Ca[Zn(OH)_3]_2{\cdot}H_2O$) and the calcium zinc ($Ca_3Zn$), which seems to be the main corrosion products of Ca-based glasses.

The FTIR spectrum of $Ca_{60}Mg_{15}Zn_{25}$ plate after corrosion test in Ringer's solution after 1 h is presented in Fig. 8a. Visible sharp peaks at 3697 cm^{-1} and at 3642 cm^{-1} are due to stretching mode of O-H vibration modes in $Mg(OH)_2$ and in $Ca(OH)_2$ [28,29]. Broad peaks at, 1455 cm^{-1}, 1395 cm^{-1}, 1082 cm^{-1} and at 852 cm^{-1} are associated with the occurrence of calcium and magnesium carbonate ($MgCO_3$ and $CaCO_3$) [30]. Additionally, FTIR spectrum also exhibited symmetric stretching vibrations from Mg-O (444 cm^{-1}) and Zn-O (544 cm^{-1}). For comparison Fig. 8b presents a spectral data obtained for $Ca_{60}Mg_{15}Zn_{25}$ sample after 3 months of keeping in the atmospheric environment. All products of the reaction were converted into calcium and magnesium carbonates. The FTIR curve revealed broad absorption peaks of CO_3^{2-} at 1395 cm^{-1}, 1082 cm^{-1} and sharp peaks at 873 cm^{-1} and 710 cm^{-1} [30,31]. For all samples (Fig. 8a,b) FTIR spectra show the bands in the range of 2700 cm^{-1} to 3600 cm^{-1}, which arise due to O-H-O stretching modes of water molecules. Additionally, the weak peak at 1645 cm^{-1} is related to O-H vibration in water.

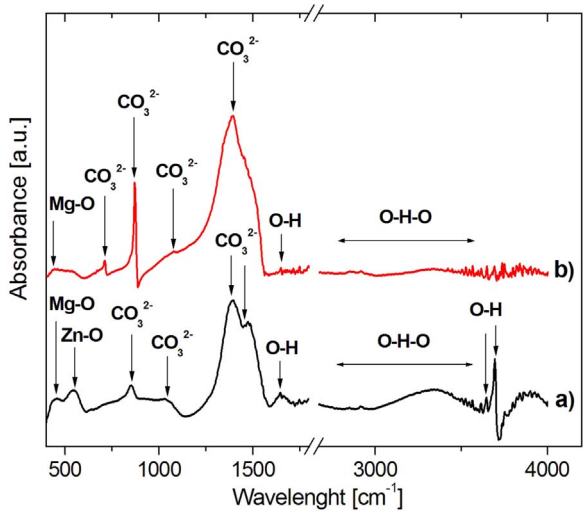

Fig. 8. ATR-FTIR spectra of $Ca_{60}Mg_{15}Zn_{25}$ amorphous alloy directly after 1 h corrosion test (a) and after 3 months of keeping in the atmospheric environment (b).

Based on the XRD and FTIR results, the main corrosion reactions in Ringer's solution (1–6) were listed below. In addition, the similar results were reported by Wang et al. [14].

$$Ca + 2H_2O \rightarrow Ca(OH)_2\downarrow + H_2\uparrow \quad (1)$$

$$Ca(OH)_2 + CO_2 \rightarrow CaCO_3\downarrow + H_2O \quad (2)$$

$$Mg + 2H_2O \rightarrow Mg(OH)_2\downarrow + H_2\uparrow \quad (3)$$

$$Mg(OH)_2 + CO_2 \rightarrow MgCO_3\downarrow + H_2O \quad (4)$$

$$Zn + 2OH^- \rightarrow ZnO\downarrow + H_2O \quad (5)$$

$$2ZnO + Ca(OH)_2 + 4H_2O \rightarrow Ca[Zn(OH)_3]_2{\cdot}2H_2O \quad (6)$$

$$Ca(OH)_2 + 2Cl^- + H_2O \rightarrow Ca^{2+} + 2Cl^- + 2OH^- \quad (7)$$

$$Mg(OH)_2 + 2Cl^- + H_2O \rightarrow Mg^{2+} + 2Cl^- + 2OH^- \quad (8)$$

$$ZnO + 2Cl^- + H_2O \rightarrow Zn^{2+} + 2Cl^- + 2OH^- \quad (9)$$

The corrosion mechanism of the studied alloy indicated that hydroxides (reactions 1 and 3) form firstly on the surface of sample. Carbonates also form (reactions 2 and 4). Due to the hydrogen evolution and dissolution by chloride ions (reactions 7–9) the corrosion layer is going to be porous without protective function. The corrosive solution reacted with unprotected metal layer (reaction 5). Nevertheless, hydroxides ($Ca(OH)_2$, $Mg(OH)_2$) and oxides (ZnO) could not stop the corrosion process and calcium zinc hydroxide hydrates (reaction 6) form. Additionally, at pH 7.4 and lower, Zn is stable and no oxide layer can be formed at surface of amorphous alloy. However, the increase of pH (due to the formation of calcium and magnesium hydroxides) causes that ZnO occurs. This result can be confirmed by the presence of the Zn-O peak identified in the FTIR spectrum (Fig. 8a).

Proposed corrosion mechanism is compatible also with the results obtained by electrochemical and XPS measurements for $Ca_{60}Mg_{15}Zn_{25}$ samples. The anodic polarization curves represent the dissolution of Ca (and other elements), while the cathodic polarization curves are focused on the hydrogen evolution by water reduction. The following electrochemical reactions can be expected for $Ca_{60}Mg_{15}Zn_{25}$ amorphous alloy (10–12):

Anodic reaction:

$$Ca \rightarrow Ca^{2+} + 2e^- \quad (10)$$

Cathodic reactions:

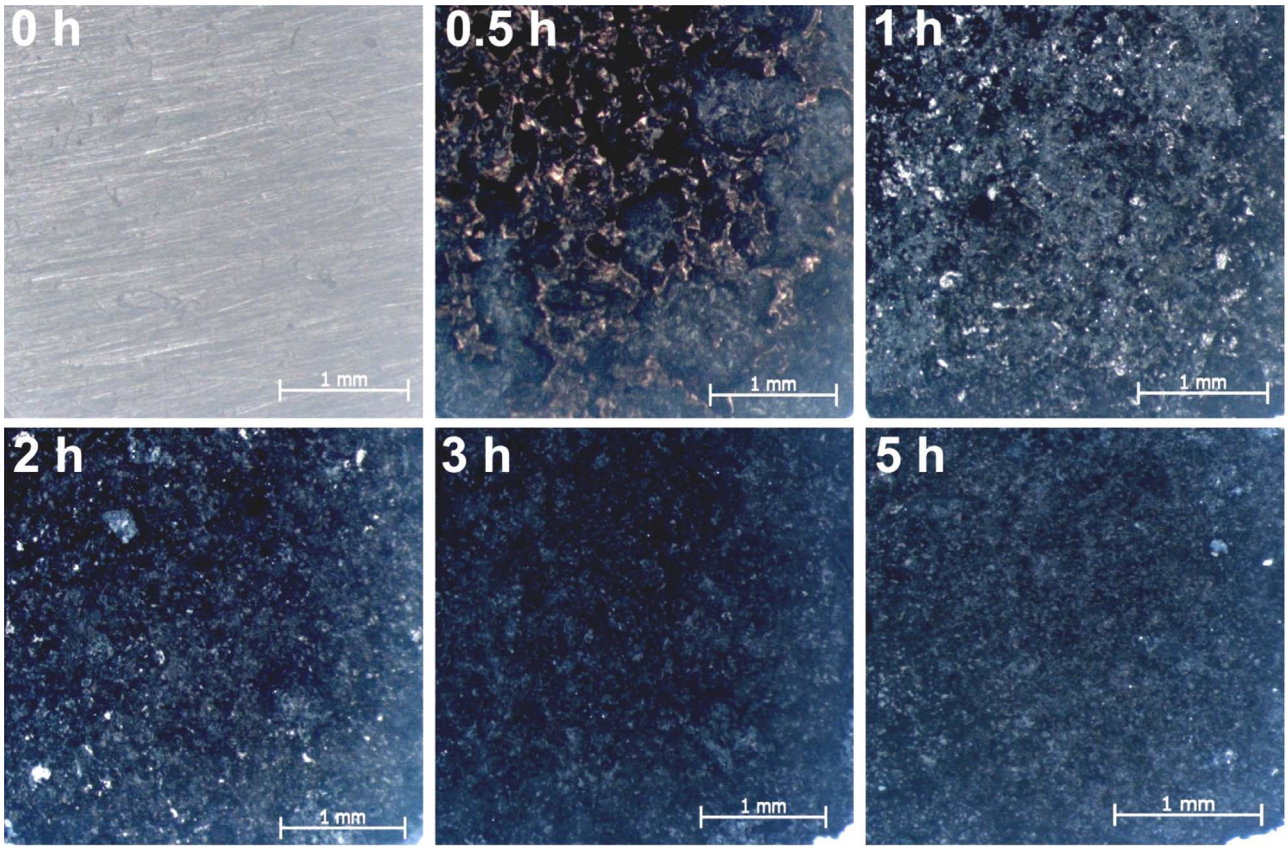

Fig. 9. Micrographs of the surface morphology of $Ca_{60}Mg_{15}Zn_{25}$ glassy plates after corrosion test in Ringer's solution.

$$2H_2O + 2e^- \rightarrow H_2 + 2OH^- \quad (11)$$

$$Ca^{2+} + 2OH^- \rightarrow Ca(OH)_2 \quad (12)$$

In Fig. 9 the effects of immersion time on the surface morphology are presented. It can be clearly seen that the corrosion of glassy alloy increases with immersion time. The immersion was performed in Ringer's solution due to more aggressive behavior. Typical surface morphologies after grinding are presented in Fig. 9 – 0 h. The characteristic scratches created by grinding were presented. After 0.5 h of immersion the single pits and filaments formed and propagated on the alloy surface. It was found that the surface of glassy plate after 1 h immersion was covered by a thick corrosion products layer, which was mainly contained calcium and oxygen species, indicating the calcium hydroxide/oxide formation. Nevertheless, this film had a very weak stability in the salt solutions (see Fig. 9 after 2 h) and the corrosion behavior was accelerated. In addition, the hydrogen evolution was observed during the immersion experiment. Therefore, the characteristic corroded regions as a result of hydrogen evolution on the specimen surface were observed (see Fig. 9 after 3 and 5 h).

For comparison, Mareci et al. [32] reported the results of the surface morphology of the MgCa samples after 1 week immersion in Ringer's solution at 37 °C. The scanning electron microscopy (SEM) was used to observe the degradation of sample surface, corrosion products formation and a non-uniform corrosion process. The energy dispersive (EDS) result confirmed that the post corroded surface contained oxygen, calcium, magnesium and chlorine. What is more, based on the results of the SEM observations Zakiyuddin and Lee [33] reported that a corrosion product layer formed on the surface of Mg and Mg-Ca alloys after the polarization tests in the simulated body fluid at 36.5 °C was not stable enough to protect the sample from the environment. They also indicated that a small amount of Ca addition caused that the corrosion product layers became less stable, and enabling more uniform corrosion process.

It is important to state that for short-term biomedical implants, the promising way to produce Ca-based alloys is to achieve an amorphous structure. However, the rapid rate of dissolution in corrosion environments due to the reactive behavior of calcium can limit their good potential as resorbable alloys. Therefore, at least two different ways are usually provided to decrease the corrosion activity of Ca alloys. The corrosion nature of Ca-based alloys was dependent on the chemical composition and the surface treatment [34].

4. Conclusions

The glassy samples have been investigated in selected isotonic fluids (multi-electrolyte and Ringer's solution) constitute a solution of salts (i.e. NaCl, KCl, $CaCl_2$, $MgCl_2$) dissolved in water with different concentration. The electrochemical measurements indicate that the corrosion current density decreases from 1062 μA/cm^2 for a sample tested in Ringer's solution to 788 μA/cm^2 for a specimen immersed in a multi-electrolyte fluid. The Ca-based alloy is rapidly reactive and the possibly initial passivation during first 1 h of immersion is not stable. The decrease of the open-circuit potential at the end of immersion indicates the further dissolution of the sample. What is more, the volume of H_2 measured in Ringer's solution is higher in comparison with the measurements provided in a multi-electrolyte fluid. The amount of evolved hydrogen increases with the increase of time. The corrosion mechanism of the studied alloy in the two selected simulated body fluids is the same, but more aggressive environment of Ringer's solution makes that the hydrogen evolution and corrosion process are more progressing. The XPS results indicate that the post-corrosive surface is mostly covered by oxides and hydroxides. Some carbonates adsorbed on the sample surface can be also identified. Furthermore, the presence of zinc can be related to zinc oxide. The X-ray and FTIR analysis of the corrosion products of the samples after 1 h of immersion confirms a formation of calcium and zinc hydroxides, calcium zinc

hydroxide hydrates as well as calcium carbonates.

Acknowledgements

The work was supported by National Science Centre under research project no.: 2013/09/B/ST8/02129.

References

[1] J.Q. Wang, J.Y. Qin, X.N. Gu, Y.F. Zheng, H.Y. Bai, J. Non-Cryst. Sol. 357 (2011) 1232–1234.
[2] M. Salahshoor, Y. Guo, Materials 5 (2012) 135–155.
[3] H.F. Li, X.H. Xie, K. Zhao, Y.B. Wang, Y.F. Zheng, W.H. Wang, L. Qin, Acta Biomater. 9 (2013) 8561–8573.
[4] Y.N. Zhang, G.J. Rocher, B. Briccoli, D. Kevorkov, X.B. Liu, Z. Altounian, M. Medraj, J. Alloy Compd. 552 (2013) 88–97.
[5] H.F. Li, Y.B. Wang, Y. Cheng, Y.F. Zheng, Mater. Lett. 64 (2010) 1462–1464.
[6] O.N. Senkov, J.M. Scott, Mater. Lett. 58 (2004) 1375–1378.
[7] P.K. Gupta, D.B. Miracle, Acta Mater. 55 (2007) 4507–4515.
[8] E.S. Park, D.H. Kim, J. Mater. Res. 19 (2004) 685–688.
[9] K. Amiya, A. Inoue, Mater. Trans. 43 (1) (2002) 81–84.
[10] Y. Li, JOM (2005) 60–63.
[11] L.L. Shi, J. Xu, E. Ma, Acta Mater. 56 (2008) 3613–3621.
[12] O.N. Senkov, J.M. Scott, J. Non-Cryst. Sol. 351 (2005) 3087–3094.
[13] J.D. Cao, N.T. Kirkland, K.J. Laws, N. Birbilis, M. Ferry, Acta Biomater. 8 (6) (2012) 2375–2383.
[14] Y.B. Wang, X.H. Xie, H.F. Li, X.L. Wang, M.Z. Zhao, E.W. Zhang, Y.J. Bai, Y.F. Zheng, L. Qin, Acta Biomater. 7 (2011) 3196–3208.
[15] J. Dahlman, O.N. Senkov, J.M. Scott, D.B. Miracle, Mater. Trans. 48 (7) (2007) 1850–1854.
[16] J.L. Li, D.Q. Zhao, M.X. Pan, W.H. Wang, J. Non-Cryst. Sol. 357 (2011) 236–239.
[17] J.V. Rau, I. Antoniac, M. Fosca, A. De Bonis, A.I. Blajan, C. Cotrut, V. Graziani, M. Curcio, A. Cricenti, M. Niculescu, M. Ortenzi, R. Teghil, Mater. Sci. Eng. C 64 (2016) 362–369.
[18] R. Babilas, K. Cesarz-Andraczke, R. Nowosielski, A. Burian, J. Mater. Eng. Perform. 23 (6) (2014) 2241–2246.
[19] R. Babilas, K. Cesarz-Andraczke, D. Babilas, W. Simka, J. Mater. Eng. Perform. 24 (1) (2015) 167–174.
[20] R. Babilas, R. Nowosielski, M. Pawlyta, A. Fitch, A. Burian, Mater. Character 102 (2015) 156–164.
[21] Z. Shi, A. Atrens, Corr. Sci. 53 (2011) 226–246.
[22] R. Nowosielski, A. Bajorek, R. Babilas, J. Non-Cryst. Sol. 447 (2016) 126–133.
[23] E. McCafferty, Corr. Sci. 47 (2005) 3202–3215.
[24] R. Babilas, A. Bajorek, W. Simka, D. Babilas, Electrochim. Acta 209 (2016) 632–642.
[25] Y. Niu, R. Cui, Y. He, Z. Yu, J. Alloy Compd. 610 (2014) 294–300.
[26] O.N. Senkov, D.B. Miracle, V. Keppens, P.K. Liaw, Metall. Mater. Trans. A 39A (2008) 1888–1900.
[27] M.L. Morrison, R.A. Buchanan, O.N. Senkov, D.B. Miracle, P.K. Liaw, Metall. Mater. Trans. A 37A (2006) 1239–1245.
[28] T.N. Ramesh, V.P. Sreenivasa, J. Mater. (2015) 1–10.
[29] M. Khachani, A. El Hamidi, M. Halim, S. Arsalane, J. Mater. Environ. Sci. 5 (2) (2014) 615–624.
[30] A.S. Kamba, M. Ismail, T.A.T. Ibrahim, Z.A.B. Zakaria, J. Nanomater. (2013) 1–9.
[31] J.D. Rodriguez-Blanco, S. Shaw, L.G. Benning, Nanoscale 3 (2011) 265–271.
[32] D. Mareci, G. Bolat, J. Izquierdo, C. Crimu, C. Munteanu, I. Antoniac, R.M. Souto, Mater. Sci. Eng. C 60 (2016) 402–410.
[33] A. Zakiyuddin, K. Lee, J. Alloy Compd. 629 (2015) 274–283.
[34] H.F. Li, Y.F. Zheng, Acta Biomater. 36 (2016) 1–20.